AIP Advances

Molecular dynamics simulation of *Y*-type nanomotors with different angles in aqueous solution

Cite as: AIP Advances **9**, 115008 (2019); https://doi.org/10.1063/1.5121642
Submitted: 26 July 2019 . Accepted: 17 October 2019 . Published Online: 14 November 2019

Zhongyu Fu, Dong Liang, Shuanlei Jiang, Pengde Zhao, Kaixin Han, and Zhen Xu

Molecular dynamics simulation of *Y*-type nanomotors with different angles in aqueous solution

Cite as: AIP Advances 9, 115008 (2019); doi: 10.1063/1.5121642
Submitted: 26 July 2019 • Accepted: 17 October 2019 •
Published Online: 14 November 2019

Zhongyu Fu,[1] Dong Liang,[1] Shuanlei Jiang,[1] Pengde Zhao,[1] Kaixin Han,[2] and Zhen Xu[1,a)]

AFFILIATIONS

[1]School of Mechanical and Automotive Engineering, Shanghai University of Engineering Science, Shanghai 201620, China
[2]School of Mechanical Engineering, University of Shanghai for Science and Technology, Shanghai 200093, China

[a)]**Electronic mail:** lcxuzhen@163.com

ABSTRACT

Nanomotors are of great importance when studying nanoelectromechanical systems that contain carbon nanotube (CNT) based nanomotors for controlled motion in water using a rotating electric field. In this paper, *Y*-type nanomotor structures based on CNTs immersed in an aqueous solution are designed, and systems with different *Y*-type structure angles are simulated using molecular dynamics. The simulation results suggest that when the rotating electric field speed is appropriate, changing the *Y*-type structure angle can adjust the hysteresis (forward and backward motion) of nanomotor rotors during rotation. Precise control over the rotation angle of the nanomotor rotor improves its working efficiency. The enclosed simulation results are an important reference when designing nanoscale propellers and complex structured nanogear systems in aqueous solutions.

I. INTRODUCTION

Recently, with the continuous application of nanotechnology in electromechanical systems, electrical equipment has begun to transition from microelectromechanical systems (MEMS) to nano-electromechanical systems (NEMS).[1,2] This miniaturized motor has produced major scientific breakthroughs in the fields of nanorobots, bio-NEMS, and nanofluids. Therefore, driving and controlling nanomotors has attracted interest from several research fields.

There have been several notable research achievements in recent years regarding nanorotary motors. For example, Man *et al.*[3] developed a nanoscale molecular tubular prototype bubble propeller-driven motor that can move a carbon nanotube (CNT) at a speed of ~60 m/s with a force of approximately 0.6 mN. Such small and fast moving nanomotors have great application value in drug delivery. Keshoju *et al.*[4] used magnetic fields to control nanowires in solution, which provided a theoretical basis for nanomachines in solution. Mallick *et al.*[5] proposed the use of dithionite ($Na_2S_2O_4$) salt for redox reactions that produced SO_2 to drive micromotors and achieve autonomous motion. The considered micromotor had a hydrodynamic diameter (D_h) of approximately 500 nm. Although nanomotors can be driven in different ways, there are few reports that discuss accurately driving and controlling nanorotary motors in aqueous solutions.

Due to the unique characteristics of CNTs,[6–13] nanorotary motors based on CNT materials have been an important research topic with some notable achievements. Li *et al.*[14] used CNTs and benzene ring molecules to form nanogears, and the related theoretical analysis showed that the transmission energy can be adjusted by changing the size of the gear teeth. This study provided a theoretical basis for complex nanogear systems. Guo *et al.*[15] reported that under an applied rotating electric field, the water molecule dipoles align with the electric field and the CNT is then forced to align its surface with the electric field. This result initiated work on self-assembly with the use of electric fields as a new tool. Wang and Král[16] reported the use of liquid pumps (nanoscale propellers) synthesized using CNTs and ruthenium molecules with molecular dynamics (MD) simulations to determine the liquid pumping rate. However, the motor system to drive nanoscale propellers has not been explicitly introduced. The design of nanomotor rotor systems

in aqueous solutions and studying the associated nanogear system to drive external loads is increasingly difficult without a clear description of the nanomotor system. Rahman *et al.*[17] designed an *I*-type molecule blade propeller and a nanogear system to drive external loads based on the principle of rotating CNTs immersed in an aqueous solution by changing the orientation of the water dipole as induced with a rotating electric field. However, this study only analyzed one nanomotor structure and nanomotor rotors with different structures are important to enhance their operating efficiency.

This work utilizes *Y*-type CNTs[18–37] with different structure angles (90°, 100°, 120°, 130°, and 150°) as multiblade rotors to drive nanomotors. The effects of the *Y*-type structure angle are explored in regard to the nanomotor rotor rotation angle, rotation speed, and cycle time. Meanwhile, *Y*-type nanomotor rotors with different angles are used to drive nanogears[38–40] and their influence on the rotation angle of the nanogear is explored.

II. MODEL AND NUMERICAL METHOD

Figure 1(a) shows a simplified schematic diagram for a nanomotor, while Fig. 1(b) shows the corresponding atomic structure diagram (θ represents the structure angle of the nanomotor rotor). A *Y*-type nanomotor rotor with structure angles θ of 90°, 100°, 120°, 130°, and 150° is combined with a (10, 10)-chirality CNT of length 2.5 nm. Two wing CNTs of chirality (6, 0) and lengths of 0.72 nm are mounted on the two sides of the *Y*-type nanomotor rotor and along the same axis as the rotating shaft. During the simulations, the two wing CNTs rotate together with the motor rotor. The two wing CNTs are placed in the center of the two fixed CNTs of chirality (8, 8) and lengths of 0.86 nm. The fixed CNTs are used as a stator of the nanomotor and do not rotate with the motor rotor. The fixed CNTs support the nanomotor shaft and ensure smooth operation of the motor rotor. In real environments, fixed CNTs require mounting on some rigid support device. Figure 1(c) indicates that the nanomotor established in Fig. 1(b) is immersed in an 8 × 8 × 5 nm^3 water tank and the number of water molecules for the Y-type nanomotor system with structure angles of 90°, 100°, 120°, 130°, and 150° are 10 030, 10 041, 10 031, 10 043, and 10 032, respectively. The nanomotor rotor can move with an applied rotating electric field of a suitable speed.

Figure 1(d) shows a simplified schematic of the nanogear system (not to scale), and Fig. 1(e) shows an atomic structure diagram corresponding to the nanogear system. Based on the nanomotor, the length of the wing CNT for the rotor side of the motor is lengthened to 1.56 nm and six benzene rings are mounted on one end as teeth for the nanogear. In addition, a CNT of chirality (6, 0) and length 1.56 nm is connected to six benzene rings to form a gear shaft to mechanically couple with the gear in contact with the nanomotor rotor. Two single-layer 9 × 9 nm^2 graphene plates are used to separate the motor rotor from the surrounding environment. The nanogear system can be used in a small aqueous solution or in a full solution environment. Figure 1(f) indicates that the nanogear system established in Fig. 1(e) is placed in a 9.2 × 9.2 × 9 nm^3 water box. During the simulations, water molecules between the two graphene plates are retained to drive the nanomotor rotor. The number of water molecules for the *Y*-type nanogear system with structure angles of 90°, 100°, 120°, 130°, and 150° are 5962, 5966, 5948, 5955, and 5956, respectively.

In the simulation process, the *XY* plane is set as the rotating plane of the nanomotor and the rotating electric fields on the *X* and *Y* axes are constructed. The functional form for the rotating electric fields are $E_x = E_t \cos(\omega t)$ and $E_y = E_t \sin(\omega t)$, where E_x and E_y are the field strengths of the combined rotating electric fields, E_t is the initial set electric field strength, ω is the angular speed of the rotating electric field, and t is the time over which the rotating electric field changes. In practice, the phase angle of the alternating current can be adjusted to construct the combined rotating electric field.[41]

The MD simulations are performed with the canonical (NVT) ensemble using the GROMACS 5.1.4 software package.[42,43] The temperature is maintained at 300 K using the v-rescale method. Periodic boundary conditions are used for all directions, and the Amber99sb-ildn force field[44] and the transferable intermolecular potential three-point (TIP3P)[45–49] water model are used in the simulations. The nonbonded parameters σ_{cc} = 0.34 nm and ε_{cc} = 0.3664 kJ mol^{-1} are the Lennard-Jones (LJ) parameters for carbon-carbon

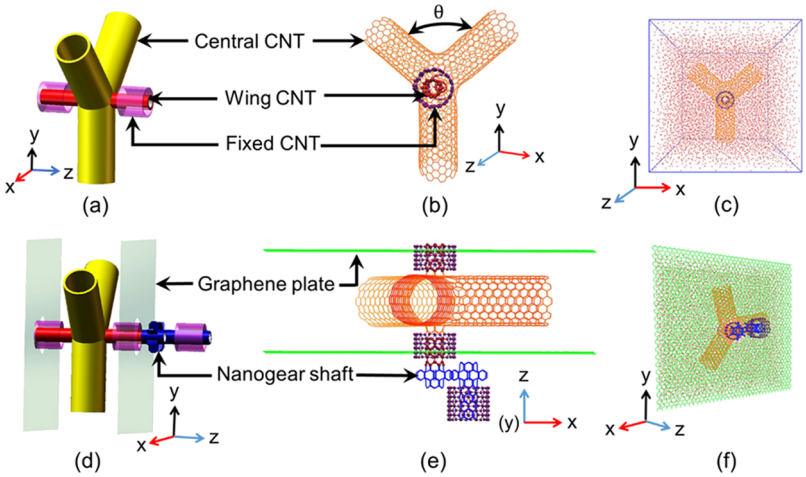

FIG. 1. (a) Schematic diagram for a simple nanomotor (not to scale), (b) atomic structure model for the *Y*-type nanomotor rotor [θ represents the structure angle of the motor rotor, yellow is the nanomotor rotor (central CNT), purple is the CNT to fix the rotor of the nanomotor, and red is the nanomotor wing CNT], (c) nanomotor structure immersed in water, (d) schematic of a simple nanogear system (not to scale), (e) atomic structure model for the nanogear system (blue is the nanogear shaft), and (f) nanogear system immersed in water.

interactions.[7,50–52] The equilibrium bond length between carbon atoms is 0.1418 nm, and the equilibrium bond angle is 120°. The harmonic potential energy function is used to constrain the bonds, where the constrained energy coefficients are 393 960 kJ mol^{-1} and 527 kJ mol^{-1} rad^{-2}, respectively. The interactions between the CNTs and the water molecules are described using the LJ potential between carbon and oxygen atoms and the LJ parameters are σ_{co} = 0.3275 nm and ε_{co} = 0.4772 kJ mol^{-1}. The role parameters used here have been widely used in many studies for CNT-water systems.[7,15,50–53] The truncated algorithm is used for LJ potential energy during the simulations with a truncation radius of 1 nm. The electrostatic interactions are subjected to the Particle-Mesh-Ewald (PME) algorithm[54,55] in which the truncation radius for the short-range action is 1 nm, the time step is 2 fs, and the data acquisition frequency is one frame per 0.5 ps.[7,18,55,56]

III. RESULTS AND DISCUSSION

Nanomotor rotors with different structure angles have the same rotating mechanism in aqueous solutions. Under the action of an electric field, the motor rotor is forced to align its surface toward the dipole orientation of the water molecules to maximize the hydrogen bonds. The generated dipole moment is because water molecules are polar with positive and negative charge centers of gravity that do not coincide. The water dipole moment is obtained as $\mu = q \times d$ and is aligned from positive to negative, where q represents the amount of charge carried by the center of the positive and negative charges and d represents the distance between the charge centers. To analyze the relationship between the dipole moment of the water molecules and the rotating electric field, we record its components along the X-, Y-, and Z-axes as p_x, p_y, and p_z, respectively. The |P| represents the mode length of the dipole moment. The Y-type rotor with a structure angle of 90° is selected for the convenience of the observations. As shown in Fig. 2(a), the average dipole strength curves for the water molecules around the Y-type nanomotor rotor are drawn along the X-, Y-, and Z-axes (p_x, p_y, and p_z, respectively). The phase difference between p_x and p_y is 90° in Fig. 2(a). The curves for the time-dependent dipole moments are satisfied with the sine and cosine curves, which are consistent with the changes in the constructed rotating electric field function, and the change in p_z is related to the defined rotating plane. Due to the changes in the electric field strength along the XY plane, the dipole orientations of the water molecules tend to coincide with the direction of the electric field. In addition, under the action of the van der Waals (vdW) forces, the dipole orientations of the water molecules during rotation deviate from the XY plane and lead to a nonzero p_z.

The lag angle θ_{Lag} represents the difference between the rotor rotating angle and the water molecule dipole rotating angle at a given same time. The relative angle is from the initial position to the rotation angle of the motor rotor. The lag angles of θ_{Lag1} and θ_{Lag2} for the Y-type motor rotors of 90° and 120° illustrate the influence of the Y-type structure angle on the motor rotor lag angle. The lag angle for the Y-type nanomotor rotor at 90° is nearly consistent during the entire rotation, as shown in Fig. 2(b). This result agrees with the work of Zasetsky *et al.*[57] When the speed of the rotating electric field is sufficiently low, the motor rotor rotation and the dipole rotation of the water molecules are nearly synchronous. For the Y-type rotor with an angle of 120°, the hysteresis angle increases with time during the rotation of the nanomotor rotor.

To more clearly reflect the variations of the lag angle with the Y-type angle, the lag angles for the Y-type rotor with different angles of 90°, 100°, 120°, 130°, and 150° are calculated and drawn when the nanomotor rotation speed is consistent with the rotating electric field step speed, as shown in Fig. 2(c). As a result, the Y-type motor rotors at 120° and 130° have a larger lag angle as time progresses. The other Y-type motor rotor speeds (angles of 90°, 100°, and 150°) are consistent with the rotating electric field. However, the lag angle of the motor rotors also increases with larger Y-type structure angles. Therefore, reducing the lag angle between the motor rotor and the water molecule dipole requires reducing the structure angle of the Y-type motor rotor, which also enhances the nanomotor rotor speed.

In Fig. 3(a), a correlation analysis of the nanomotor rotor immersed in an aqueous solution is performed to further analyze the cause of the Y-type nanomotor rotor hysteresis with structure angles of 120° and 130°. The dipole moment of the circumferentially driven rotor for the entire nanomotor rotor system is

$$D \sin\alpha = D_1 \sin\alpha_1 + D_2 \sin\alpha_2 + D_3 \sin\alpha_3, \quad (1)$$

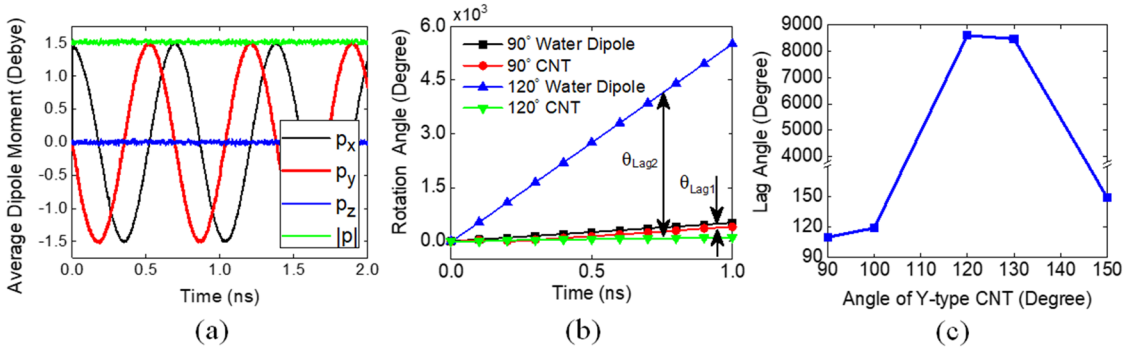

FIG. 2. (a) Curves for the average dipole moment of the water molecules in the nanomotor system with time when the rotating electric field strength is 1 v/nm with a speed of 8.75 × 10^{10} rpm, (b) the dipole and the motor rotor rotation angle curves for the Y-type motor rotors of 90° and 120° with time, and (c) curve for the lag angle for different Y-type nanomotor rotor angles.

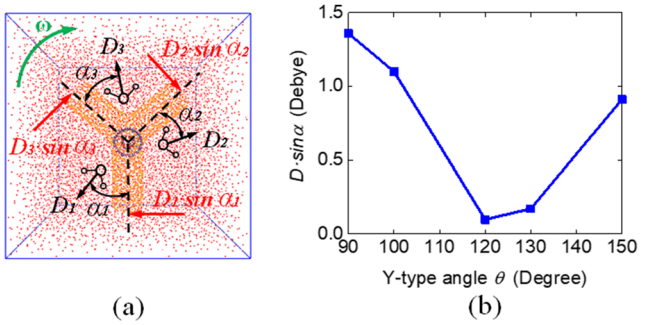

FIG. 3. (a) Mechanical analysis diagram for the *Y*-type nanomotor rotor in water and (b) a curve for the circumferential tangential force of the nanomotor rotor with the structure angle.

where the average dipole moment D represents the vector sum of D_1, D_2, and D_3; and α_1, α_2, and α_3 represent the angles between each branch the average dipole moment of the water molecules and each branch axis, respectively. The angle α is equivalent to the angle between the overall average dipole moment D and the Y-axis. It can be seen from Fig. 2(a) that the magnitude of the average dipole moment D for the water molecules is related to the E_t setting of the rotating electric field. In this study, the same set of rotating electric fields is used for different Y-type structure angles. Therefore, the average dipole moments for different Y-type structure angles are the same. Thus, the main factor that affects the rotation of the rotor is the angle α between the average dipole moment of the water molecules and the axis of the CNTs. Based on the simulation results, the angles between the average dipole moment of the water molecules for the Y-type structure angles of 90°, 100°, 120°, 130°, and 150° and the CNT axis are 67°, 53°, 4°, 7°, and 39°, respectively. As can be seen from the graph in Fig. 3(b), the Y-type structure angles of 120° and 130° provide a lower circumferential force of rotation than the structure angles of 90°, 100°, and 150°. This causes the hysteresis effect during rotation to be more obvious.

As shown in Fig. 4(a), when there is no forward and backward motion (see Movie S1 in the supplementary material), the rotating angles for the Y-type structure angles of 120° and 130° are less than those for the structure angles of 90°, 100°, and 150°. This is mainly because the structure angles of 120° and 130° produce a large lag angle during the rotating process, which prolongs the period of the nanomotor rotor. This result is confirmed in the outcome of Fig. 2(c). In addition, according to Fig. 4(a) with different speed orders, a rotating electric field is required to provide a sufficiently large rotating speed to allow the motor rotor to rotate for Y-type structure angles of 120° and 130°. This result indicates that during the rotation of the nanomotor rotor with structure angles of 120° and 130°, the angle between the water molecule dipole moment around the nanomotor rotor and the rotor axis is small, which results in a small circumferential tangential force. Therefore, a greater electric field speed is required to drive the nanomotor rotor.

The average speed of the motor rotor over one cycle is used to represent the motor rotor speed. The Y-type motor rotor speed curves for different structure angles increase and then decrease, as shown in Fig. 4(b). This is because the speed of the rotating electric field is too fast for the nanomotor rotor to "lock" onto the rotating electric field. Therefore, the nanomotor rotor will exhibit forward and backward motion during the rotation process (see Movie S2 in the supplementary material). As reported by Rahman *et al.*[17] and Zasetsky,[57] not all rotating electric field speeds can be used to drive a nanomotor rotor. In addition, although the Y-type structure nanomotor rotors with structure angles of 120° and 130° are driven with higher electric field speeds, it is still not sufficient to produce a large increment. The speeds of the motor rotors with structure angles 120° and 130° are not as good as those for structure angles of 90°, 100°, and 150°.

From the graph of the interaction energy between the motor rotor and the aqueous solution [Fig. 4(c)], the interaction energies for the Y-type motor rotor with structure angles of 90°, 100°, and 150° are overall larger than for the structure angles of 120° and 130°. The former motor rotors can be positioned over a short time. Additionally, for the Y-type structure angles of 90°, 100°, and 150°,

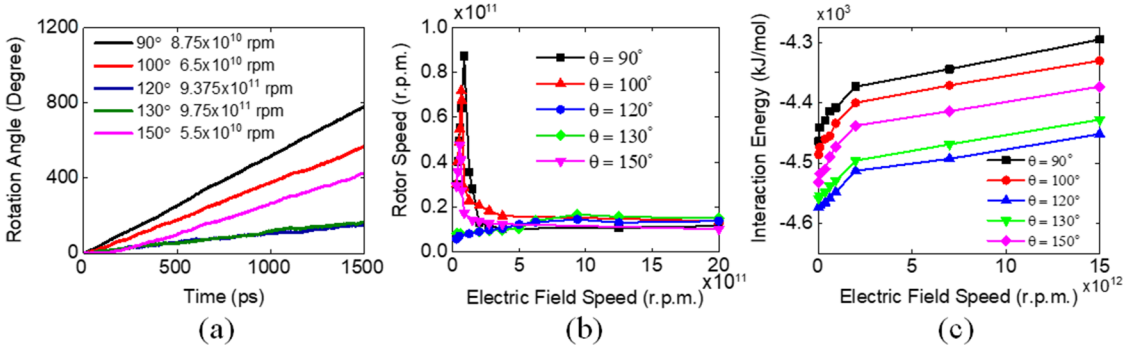

FIG. 4. (a) Changes in the rotation angle for different *Y*-type structure angles with respect to time without forward and backward motion when the rotating electric field strength is 1 V/nm, (b) rotor speed of the *Y*-type structure nanomotors with different structure angles as functions of the rotating electric field speed when the field strength is 1 V/nm, and (c) the interaction energy of the *Y*-type rotors with different structure angles between the motor rotor and the aqueous solution as functions of the rotating electric field speed when the field strength is 1 V/nm and the nanomotor rotor does not produce forward and backward motion.

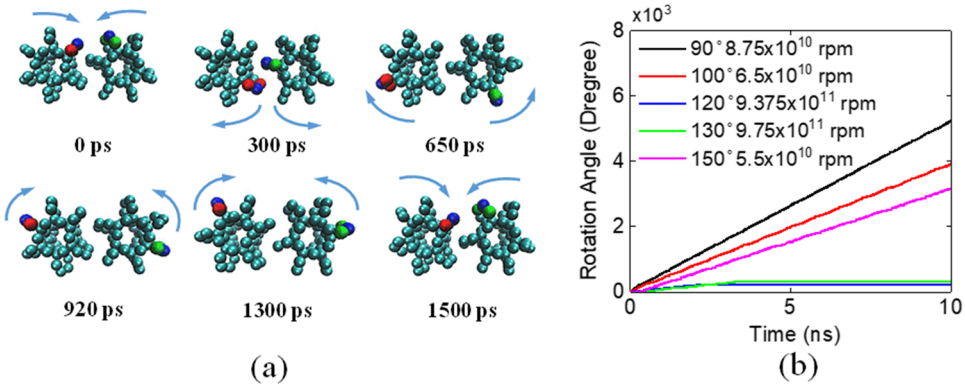

FIG. 5. (a) Snapshots of the nanogear at different positions in a cycle are taken (the nanogear marked is red and blue is the driving wheel, and the nanogear marked with green and blue is the driven wheel) when the rotating electric field strength is 1 v/nm, the electric field speed is 8.75×10^{10} rpm, and the motor rotor does not move forward and backward; and (b) curves for the nanogear rotating angle with time when the rotating electric field strength is 1 V/nm and different *Y*-type structure angles do not produce forward and backward motion.

the water molecules around the rotor have different orientation times. A *Y*-type motor rotor with a high rotating electric field speed results in water molecules around the motor rotor orienting themselves over a relatively short time. These results demonstrate that the orientation of water molecules is affected by the rotating electric field, which corresponds to the results of Winarto *et al.*[51] Therefore, when designing a *Y*-type nanomotor, adjusting the *Y*-type structure angle to reduce the orientation time for the water molecules should be considered so that the motor rotor can be positioned over a shorter time.

Based on the *Y*-type nanomotor rotor studied in Sec. II, we connected six benzene molecules to the wing CNTs on the rotor side of the motor as the nanogear teeth. The two nanogears are mechanically coupled to the benzene teeth. To clearly illustrate the engagement of the two gears, snapshots at different positions in a cycle are shown in Fig. 5(a) (see Movie S3 in the supplementary material). Figure 5(b) shows that the nanogears driven by different *Y*-type structure angles of 90°, 100°, and 150° are nearly consistent with the rotating angle of the nanomotor rotor. However, for nanogears driven by the *Y*-type nanomotor rotors with structure angles of 120° and 130°, the rotating angles remain unchanged for a period of time, and the motions are stopped. Comparing Figs. 2(b) and 2(c), it is seen that for the structure angles of 120° and 130°, when the lag angle is small, the nanomotor rotor can rotate. When the lag angle is large, the nanomotor rotor cannot lock onto the rotating electric field speed, which results in a stagnant state. Therefore, when designing a nanogear system, the lag angle should be minimized to improve the working efficiency of the entire gear transmission system.

With the continuous development of NEMS, ultrahigh-speed, easy-to-assemble and low-friction *Y*-type nanogear systems in water have attracted a lot of researchers' interest. The output speed of the *Y*-type nanogear system is lower than that of the *I*-type nanogear system studied by Rahman *et al.*[17] This is mainly caused by the circumferential force of the *Y*-type rotor being smaller than the circumferential force of the *I*-type rotor. However, the rotation effect of the *Y*-type nanogear system is consistent with the nanogear system designed by Rahman *et al.* The design of *Y*-shaped nanogears at different angles has led to a further understanding of gears at the microscopic scale.

IV. CONCLUSIONS

Based on the results of the MD simulations, with an appropriate rotating electric field speed, *Y*-type nanomotor rotors can rotate, and *Y*-type nanogear systems based on the motor rotor can be coupled normally. For *Y*-type nanomotor rotors with different structure angles, adjusting the circumferential force of the *Y*-type nanomotor rotor by changing the structure angle θ allows generating a large rotational speed under the same electric field conditions. In addition, when designing a nanogear system, it is necessary to consider changes in the lag angle. When the lag angle is sufficiently large, the nanomotor rotor locks onto the pace of the rotating electric field, which eventually causes the nanogear system to enter a stagnant state. These findings for the *Y*-type nanomotor rotors with different structure angles helps accomplish precise control of nanogear systems by changing the structure angle. This provides a theoretical basis for research into new nanofluid machines, nanorotary pumps with complex structures, and a nanomechanical arm with multiple degrees of freedom.

SUPPLEMENTARY MATERIAL

See the supplementary material for Movie-S1.mp4, Movie-S2.mp4, and Movie-S3.mp4 (https://github.com/fzypaper/hello-world.git).

ACKNOWLEDGMENTS

This work was supported by the National Science Foundation of China (Grant No. 11604203).

REFERENCES

[1] X. Zhang, Q. Guo, and D. Cui, Sensors **9**(2), 1033–1053 (2009).
[2] M. Guix, C. C. Mayorga-Martinez, and A. Merkoçi, Chem. Rev. **114**(12), 6285–6322 (2014).
[3] V. H. Man, M. S. Li, J. Wang, P. Derreumaux, and P. H. Nguyen, J. Chem. Phys. **151**, 024103 (2019).
[4] K. Keshoju, H. Xing, and L. Sun, Appl. Phys. Lett. **91**(12), 123114 (2007).
[5] A. Mallick, D. Lai, and S. Roy, New J. Chem. **40**, 1057–1062 (2016).
[6] V. N. Popov, Mater. Sci. Eng.: R: Rep. **43**(3), 61–102 (2004).
[7] J. Zou, B. Ji, X. Feng, and H. Gao, Nano Lett. **6**(3), 430–434 (2006).

[8]X. Gong, J. Li, K. Xu, J. Wang, and H. Yang, J. Am. Chem. Soc. **132**(6), 1873–1877 (2010).
[9]K. Wu, B. Zhou, P. Xiu, W. Qi, R. Wan, and H. Fang, J. Chem. Phys. **133**(20), 204702–204707 (2010).
[10]P. G. Collins, M. S. Arnold, and P. Avouris, Science **292**(5517), 706–709 (2001).
[11]Y. Liu, Q. Wang, T. Wu, and L. Zhang, J. Chem. Phys. **123**(23), 234701 (2005).
[12]H. M. Duong, D. V. Papavassiliou, K. J. Mullen, B. L. Wardle, and S. Maruyama, J. Phys. Chem. C **112**(50), 19860–19865 (2008).
[13]K. Cai, J. Yu, J. Shi, and Q. H. Qin, Sci. Rep. **6**, 27338–27347 (2016).
[14]Y. Li, Y. Liu, Q. Wang, and Q. Sun, J. Comput. Theor. Nanosci. **7**(8), 1457–1461 (2010).
[15]X. Guo, J. Su, and H. Guo, Soft Matter **8**(4), 1010–1016 (2012).
[16]B. Wang and P. Král, Phys. Rev. Lett. **98**(26), 266102–266105 (2007).
[17]M. M. Rahman, M. M. Chowdhury, and M. K. Alam, Small **13**(19), 1603978 (2017).
[18]G. Hummer, J. C. Rasaiah, and J. P. Noworyta, Nature **414**(6860), 188–190 (2001).
[19]L. P. Biró, Z. E. Horváth, G. I. Márk, Z. Osváth, A. A. Koós, A. M. Benito, W. Maser, and P. Lambin, "Carbon nanotube Y junctions: growth and properties," Diamond Rel. Mat. **13**(2), 241–249 (2004).
[20]I. Zsoldos, J. Geom. Phys. **61**(1), 37–45 (2011).
[21]S. Iijima, P. M. Ajayan, and T. Ichihashi, Phys. Rev. Lett. **69**(21), 3100–3103 (1992).
[22]P. Nagy, R. Ehlich, L. P. Biró, and J. Gyulai, Appl. Phys. A: Mater. Sci. Process. **70**(4), 481–483 (2000).
[23]M. Terrones, F. Banhart, N. Grobert, J. C. Charlier, H. Terrones, and P. M. Ajayan, Phys. Rev. Lett. **89**(89), 075505 (2002).
[24]Z. Qin, Q.-H. Qin, and X.-Q. Feng, Phys. Lett. A **372**(44), 6661–6666 (2008).
[25]M. Palma, W. Wang, E. Penzo, J. Brathwaite, M. Zheng, J. Hone, C. Nuckolls, and S. J. Wind, J. Am. Chem. Soc. **135**(23), 8440–8443 (2013).
[26]C. Papadopoulos, A. Rakitin, J. Li, A. S. Vedeneev, and J. M. Xu, Phys. Rev. Lett. **85**(16), 3476–3479 (2000).
[27]A. N. Andriotis, M. Menon, D. Srivastava, and L. Chernozatonskii, Phys. Rev. Lett. **87**(6), 066802 (2001).
[28]L. P. Biró, R. Ehlich, Z. Osváth, A. Koós, Z. E. Horváth, J. Gyulai, and J. B. Nagyc, Diamond Relat. Mater. **11**(3-6), 1081–1085 (2002).
[29]V. Meunier, M. B. Nardelli, J. Bernholc, T. Zacharia, and J.-C. Charlier, Appl. Phys. Lett. **81**(27), 5234 (2002).
[30]Z. Osváth, A. A. Koós, Z. E. Horváth, J. Gyulai, A. M. Benito, M. T. Martínez, W. K. Maser, and L. P. Biró, Chem. Phys. Lett. **365**(3-4), 338–342 (2002).
[31]D.-H. Kim, J. Huang, B. K. Rao, and W. Choi, J. Appl. Phys. **99**(5), 056106 (2006).
[32]D. Fua, X. Zeng, J. Zou, H. Qian, X. Li, and X. Xiong, Mater. Chem. Phys. **118** (2-3), 501–505 (2009).
[33]A. N. Andriotis, M. Menon, D. Srivastava, and L. Chernozatonskii, "Transport properties of single-wall carbon nanotube Y junctions," Phys. Rev. B **65**(16), 165416 (2002).
[34]Y. C. Choi and W. Choi, Carbon **43**(13), 2737–2741 (2005).
[35]J. Park, C. Daraio, S. Jin, P. R. Bandaru, J. Gaillard, and A. M. Rao, Appl. Phys. Lett. **88**(24), 243113 (2006).
[36]W. Choi, D. Kim, Y. C. Choi, and J. Huang, JOM **59**(3), 44–49 (2007).
[37]P. R. Bandaru, C. Daraio, S. Jin, and A. M. Rao, Nat. Mater. **4**(9), 663–666 (2005).
[38]J. Han, A. Globus, R. Jaffe, and G. Deardorff, Nanotechnology **8**(3), 95–102 (1997).
[39]E. Taşcı, O. B. Malcıoğlu, and Ş. Erkoç, Fullerenes, Nanotubes, Carbon Nanostruct. **16**(1), 30–39 (2008).
[40]P. Yang and H. Zhang, Tribol. Int. **41**(6), 535–541 (2008).
[41]D. L. Fan, F. Q. Zhu, R. C. Cammarata, and C. L. Chien, Phys. Rev. Lett. **94**(24), 247208 (2005).
[42]B. Hess, C. Kutzner, D. V. D. Spoel, and E. Lindahl, J. Chem. Theory Comput. **4**(3), 435–447 (2008).
[43]S. Pronk, S. Páll, R. Schulz, P. Larsson, P. Bjelkmar, R. Apostolov, M. R. Shirts, J. C. Smith, P. M. Kasson, D. V. D. Spoel, B. Hess, and E. Lindahl, Bioinformatics **29**(7), 845–854 (2013).
[44]M. Orsi, Chem. Biol. Technol. Agric. **1**(1), 10 (2014).
[45]D. Braun, S. Boresch, and O. Steinhauser, J. Chem. Phys. **140**(6), 064107 (2014).
[46]D. J. Price and C. L. Brooks, J. Chem. Phys. **121**(20), 10096–10103 (2004).
[47]H. Dominguez, Chem. Phys. Lett. **651**, 92–96 (2016).
[48]P. T. Kiss and A. Baranyaia, J. Chem. Phys. **134**(5), 054106 (2011).
[49]W. L. Jorgensen, J. Chandrasekhar, J. D. Madura, R. W. Impey, and M. L. Klein, J. Chem. Phys. **79**(2), 926–935 (1983).
[50]Z. Xu, C. Wang, N. Sheng, G. Hu, Z. Zhou, and H. Fang, J. Chem. Phys. **144**(1), 014302 (2016).
[51]Winarto, D. Takaiwa, E. Yamamoto, and K. Yasuoka, Phys. Chem. Chem. Phys. **18**(48), 33310–33319 (2016).
[52]M. M. Rahman, M. M. Chowdhury, and M. K. Alam, in *International Conference on Electrical and Computer Engineering* (IEEE, 2015).
[53]C. D. Daub, D. Bratko, T. Ali, and A. Luzar, Phys. Rev. Lett. **103**(20), 207801 (2009).
[54]D. Barash, L. Yang, X. Qian, and T. Schlick, J. Comput. Chem. **24**(1), 77–88 (2003).
[55]T. Darden, D. York, and L. Pedersen, J. Chem. Phys. **98**(12), 10089–10092 (1993).
[56]X. Gong, J. Li, H. Lu, R. Wan, J. Li, J. Hu, and H. Fang, Nat. Nanotechnol. **2**(11), 709–712 (2007).
[57]A. Y. Zasetsky, Phys. Rev. Lett. **107**(11), 117601 (2011).